


## ARTICLE

# Effect of chain extender on the morphology, thermal, viscoelastic, and dielectric behavior of soybean polyurethane

Diana Favero<sup>1</sup> | Victória Marcon<sup>1</sup> | Carlos A. Figueroa<sup>1</sup> | Clara M. Gómez<sup>2</sup> | Ana Cros<sup>2</sup> | Nuria Garro<sup>2</sup> | Maria J. Sanchis<sup>3</sup> | Marta Carsí<sup>4</sup> | Otávio Bianchi<sup>1,5</sup> 

<sup>1</sup>Programa de Pós-graduação em Engenharia e Ciência dos Materiais – PGMAT, Universidade de Caxias do Sul, Caxias do Sul, Brazil

<sup>2</sup>Instituto de Ciencia de los Materiales (ICMUV), Universidad de Valencia, Valencia, Spain

<sup>3</sup>Department of Applied Thermodynamics, Institute of Electric Technology, Universitat Politècnica de València, Valencia, Spain

<sup>4</sup>Department of Applied Thermodynamics, Instituto de Automática e Informática Industrial, Universitat Politècnica de Valencia, Valencia, Spain

<sup>5</sup>LAPol-Departamento de Engenharia dos Materiais, Universidade Federal do Rio Grande do Sul, Porto Alegre, Brazil

## Correspondence

Otávio Bianchi, Programa de Pós-graduação em Engenharia e Ciência dos Materiais – PGMAT, Universidade de Caxias do Sul, Getúlio Vargas, 1130 – CEP 95070-560, Caxias do Sul, Brazil.  
Email: otavio.bianchi@gmail.com

## Funding information

National Council for Scientific and Technological Development (CNPq), Grant/Award Number: 306086/2018-2; Coordenação de Aperfeiçoamento de Pessoal de Nível Superior (CAPES); Spanish Ministerio de Economía y Competitividad, Grant/Award Number: RTI2018-093711-B-100; AEI/FEDER, UE, Grant/Award Number: ENE2016-79282-C5-3-R; Sindicato das Indústrias de Material Plástico do Nordeste Gaúcho (SIMPLÁS)

## Abstract

The objective of this work was to determine the influence of different chain extenders (CEs) on the morphology, thermal, viscoelastic, and dielectric properties of soybean polyurethane (PU). The PU with ethane-1,2-diol showed a more organized structure, which was attributed to the smaller amount of methylene groups ( $-\text{CH}_2-$ ) and the shorter distance between the hydrogen bonds. While, PUs with dipropylene glycol, the free volume increased due to the less effective interactions formed between the hard and soft domains. The  $\alpha$ ,  $\beta$ , and  $\gamma$  transitions dipolar by conductive process, are probably associated with (a) local motions of the main chain, (b) the smaller groups rotation motions in the fatty acid chains in the soft phase, and (c) the  $-\text{CH}_2-$  group rotation motion in the amorphous region. The phase-separated morphology is most evident at high temperatures due to the Maxwell–Wagner–Sillars interfacial polarization process.

## KEYWORDS

renewable polymers, dielectric properties, soy-based polyol, polyurethane, structure-property relationships

## 1 | INTRODUCTION

Soybean polyurethanes (PUs) stand out for exhibiting excellent resistance to hydrolysis, good biocompatibility, and macromolecular design flexibility. PUs obtained from soybean oil polyol (SOP) is an excellent total or partial alternative to the petroleum-derived polyols substitution in the polymer industry. The soybean PUs final properties can be easily tuned for applications ranging from thermoplastic or thermosetting polymers such as thermal insulation foams or elastomers.<sup>1–3</sup> The SOP is considered a “green” material due to its renewable characteristics, and it is typically used in the soft domain phase composition. The hard domain is usually formed by a chain extender (CE) and a di-isocyanate (aromatic or aliphatic).<sup>4</sup> CEs such as polyfunctional low molecular weight alcohols may also be added to the formulation to obtain PUs with different physicochemical characteristics.<sup>1,3,5</sup>

Besides, the SOP can be obtained by several methods. The most consolidated and industrially used one is the epoxidation, which is generated in two stages. Thus, the hydroxyl groups form through the epoxide-ring opening during microwave-assisted alcoholysis reaction. The SOP preparation time reduction is the main advantage of this method.<sup>6,7</sup> The SOP obtained by the epoxidation method followed by epoxide-ring opening tends to show functionality greater than 2.0, due to the initial amount of double bonds the soybean oil characteristic.<sup>6,8,9</sup> However, it is essential to combine CEs to adjust the PUs properties. The CEs functionality and amount can increase chemical crosslinking and, thus, restrict physical crosslinking such as the motion of the macromolecular chain in the soft block, due to hydrogen bonds.<sup>10</sup> The PUs properties are strongly dependent on the intra- and interchain interactions, such as hydrogen bonds between the polar chain groups, mainly nitrogen groups NH (proton donors) and carbonyl C=O (electron donors) present in the urethane group and polyols.<sup>11</sup> The size, distribution, and hard and soft domains morphology in PUs are dependent on the hydrogen bond distribution in the copolymer.

Consequently, the phase separation degree is influenced by the nature of PU constituents and their interactions. In general, there is a higher phase separation degree in the PUs with an increased hydrogen bond number formed in the urethane group.<sup>1</sup> A considerable mixed-phase amount is observed when there is high interaction between the hard and soft domains. Thus, the hard and soft domain amount formed is also variable due to the hydrogen bonds distribution in the copolymer. Petrovick et al.<sup>2</sup> obtained soybean PUs with the use of diphenylmethane 4,4' diisocyanate (MDI) and CEs: ethylene-1,2-glycol (EG) and butane-1,4-diol (BDO) with

40 wt% hard domain ([NCO]/[OH] = 1.1/1.0 mol/mol molar ratio). The dynamic mechanical behavior showed  $\alpha$ -transition at 60°C associated with the fatty acids chain segmental motion and  $\beta$ -transition at –60°C associated with the smaller chain rotation.

Overall,  $\alpha$ -relaxation of the PUs is attributed to long-range motions of conformational changes in the main chain of soft phases, while the  $\beta$ -relaxation is derived from local motions of the main chain.<sup>12</sup> However, segmental relaxations depend on the characteristics of the precursor monomers that will form the polymer.<sup>13</sup> Based on the Petrovick et al.<sup>2</sup> work, we believe that, as seen in the vast majority of olefinic polymers, the type Schatzki transition must be observed it is originated from the hindered methylene repeating unit rotation, [–CH<sub>2</sub>–], in diols in the main chain of amorphous soft phases. Oprea et al.<sup>14</sup> synthesized castor PUs with 1.6 hexamethylene diisocyanate (HDI) and 1.4 butanediol as CE. They observed that the hydrogen bonds between urethane groups contribute to control the macromolecular mobility and that the relaxation phenomena are dependent on temperature–frequency. Hydrogen bonding anchors the hard domain in the soft phase and inhibits conformational rotation of the main chain.

PUs based on vegetable oil have a heterogeneous phase morphology. This phase separation phenomenon comes about with the hard domain formation dispersed in the amorphous matrix and, the size of the soft domain is related to the hard/soft content. Overall, the domain size is in the submicron and nanometer scale. Soybean PUs presents mechanical and thermal properties competitive with PUs based on petrochemistry.<sup>15</sup> However, the scientific knowledge of the different effects of the CEs in the soybean PUs microstructure is still small.

Similarly, research concerning the phase separation degree, the nature of the formed hydrogen bonds (inter- and intra-molecular interactions), and the microphase composition, that establishes fundamental correlations between soybean PUs structure-properties, is quite limited.<sup>1</sup> Overall, the phase separation degree is influenced by the characteristics of the domain blocks formed (hard and soft) during PU syntheses, such as miscibility, length, chemical composition, and weight ratio.<sup>16</sup> The Fourier transform infrared (FTIR) is generally sensitive in the carbonyl region at 1741 cm<sup>–1</sup> in which occurs phase separation and hydrogen bond behavior. Accordingly, when the carbonyl group is associated with hydrogen bonds, the unfolding of the carbonyl groups band is observed.<sup>11,16</sup> Furthermore, other complementary techniques may also aid in understanding the biobased PUs phase separation.<sup>2,17,18</sup> However, the most significant difficulty is finding literature with the extensive characterization of this material type.

In this article, the main objective was to evaluate the effect of CEs on morphology, hydrogen bonding density, viscoelastic, thermal, dielectric properties of soybean PUs. Given future applications, it is of crucial importance to evaluate these properties due to their impact on the final characteristics of polymers obtained from SOP.<sup>2</sup>

The use of different CES alters the hydrogen bond density, and consequently the PU morphology. Thus, it was possible to show with greater clarity the relationship between the structure-properties of biobased PUs. The methodology and results shown can assist in the structural understanding for other studies of biobased PU.

prevent bubbles formation, 1.1:1.0 OH:NCO molar ratio. Here, PUs with butane-1,4-diol (BDO), ethane-1,2-diol (MEG), and (2-hydroxypropoxy)propane-2-ol (DPG) used as CEs were prepared in the same way. After homogenization, the samples were then placed in a Teflon coated petri dish in an oven at 60°C for 96 h. Finally, the samples were placed in a desiccator with silica gel to avoid moisture absorption from the environment. To evaluate the CE effect a sample was prepared without its use. This was called PU-PURE composed only of SOP and MDI. The hard domain (HS) content for each PU with different CE, was calculated with Equation (1)<sup>5</sup>:

$$\text{wt}(\%)\text{HS} = \frac{\text{molar equivalent MDI} + \text{molar equivalent CE}}{\text{molar equivalent MDI} + \text{molar equivalent CE} + \text{molar equivalent SOP}} \quad (1)$$

## 2 | EXPERIMENTAL SECTION

### 2.1 | Materials

The following raw materials were used in the PU synthesis: SOP was obtained from soybean oil, by the same research group,<sup>4</sup> with acid index 0.32 mg KOH/g, saponification index 150.0 mg KOH/g, hydroxyl number 190 mg KOH/g, molecular weight 1463 g/mol (GPC measurements in THF), functionality of 4.98, viscosity at 60°C  $2.4 \times 10^{-5}$  mPa/s, water content 0.17 wt% and glass transition  $-80^\circ\text{C}$  by dielectric measurements. 4,4'-diphenylmethane-diisocyanate (MDI; CAS number 101-68-8) with a free isocyanate index of  $33.49 \pm 0.07$  wt % and functionality of 2.0 was supplied by BASF (MDI). Ammonia aqueous solution (25 wt%) was purchased Dinâmica (Brazil). The CEs used were: butane-1,4-diol (BDO; CAS number 110-63-4) was purchased BASF, ethane-1,2-diol (MEG; CAS number 107-21-1) was purchased Sigma-Aldrich, and (2-hydroxypropoxy)propane-2-ol (DPG; CAS number 2526-71-8) was purchased Down Brazil. The CEs were distilled before use.

### 2.2 | Synthesis of renewable PUs with different chain extender

PUs with different CEs were synthesized, without any catalyst, by one-step bulk polymerization with approximately 39 wt% hard domain. First, the MDI was heated at 45°C for 5 min. Then the SOP, MDI, and CE were mixed for approximately 40s, under slow stirring, to

### 2.3 | Physico-chemical characterization

The chemical groups formed during PU polymerization were evaluated by FTIR spectroscopy (Perkin-Elmer Spectrum 400 spectrometer instrument) in attenuated total reflection (ATR; diamond crystal at 45°) mode. The samples were scanned 32 times, in the range from 4000 to 450  $\text{cm}^{-1}$  at 2  $\text{cm}^{-1}$  resolution. The hydrogen bonding degree and the hard domain amount dispersed in the soft phase were computed by mathematical deconvolution of the signal according to the literature.<sup>11,12</sup>

The CEs content effect on the crosslinking degree of the PUs was estimated from the gel content (GC) determined according to a procedure based on the ASTM D2765 standard. Samples (approximately 0.3 g) were cut from the PUs films, weighed, and then put into a Soxhlet extractor with dimethylformamide. After extraction, all samples were dried at 60°C for 48 h. The GC was estimated from Equation (2) as follows<sup>2</sup>:

$$\text{GC (wt}\%) = \frac{w_f}{w_i} 100 \quad (2)$$

where  $w_f$  is the final sample weight after drying, and  $w_i$  is the initial weight.

Solid viscoelastic properties, as well as molecular motions involved in the determination of the glass transition temperature ( $T_g$ ) in all PUs were obtained from  $\tan \delta$  peaks of dynamic mechanical analysis (DMA). DMA analysis was performed in TA Instruments (2890 model) using tensile film clamp mode in a viscoelastic region condition (1 Hz, 20  $\mu\text{m}$ , and a heating rate at 3°C/min).

Samples with 15.0 mm length  $\times$  6.0 mm width  $\times$  0.5 mm dimensions were used. All experiments were performed in triplicate. Also,  $\gamma$ -,  $\beta$ - and  $\alpha$ -transitions, the last related to the glass transition temperature, were obtained by dielectric relaxation spectroscopy (DRS).

DRS measurements in the frequency range from  $5 \times 10^{-2}$  to  $3 \times 10^6$  Hz were performed using Novocontrol Broadband Dielectric Spectrometer (Hundsagen, Germany) consisting of an Alpha analyzer. The measurements were performed in  $N_2$  inert atmosphere from 140 to 160°C in steps of 5°C using the temperature control system a Novocontrol Quatro cryosystem, with an accuracy of  $\pm 0.1^\circ\text{C}$  during each sweep in frequency. Samples with disc-shaped about 0.1 mm thickness and 40 mm diameter were used. Before carrying out the measurements, to avoid the increase in conductivity due to water, the samples were placed at 50°C in a vacuum oven for 24 h, until reaching a constant weight.

The experimental uncertainty was better than 5% in all cases. Classically, four relaxation functions have been developed and widely applied to describe dielectric relaxation, however the most general because of its ability to model a broad and asymmetric distribution of relaxation times is the Havriliak–Negami (HN) function. For this reason, the characterization of the dielectric spectra, in the zone corresponding to the Schatzki dipolar process, was carried out using the HN empirical model.<sup>6</sup> This model enables a complete description of a real (non-Debye) relaxation process in a polymer. It is the most general model because of its ability to model a broad and asymmetric distribution of relaxation times. The HN fitting parameters for each sample were determined at several temperatures from a multiple nonlinear regression analysis of the loss permittivity ( $\epsilon''$ ) experimental data. The secondary relaxation strength was expressed in the Onsager–Fröhlich–Kirkwood (OFK) model terms.<sup>7,8</sup>

The Schatzki region was identified using the differential scanning calorimetry (DSC). The analysis was carried out in a Netzsch DSC 204 Phoenix instrument, with a sample of 9–10 mg under the nitrogen atmosphere (50 ml/min). The melting temperature and enthalpy were calibrated with indium, tin, bismuth, and zinc standards. Under these conditions, the PUs were analyzed from  $-180$  to  $150^\circ\text{C}$  at  $20^\circ\text{C}/\text{min}$  scanning rate.

The PUs surface phase morphologies were evaluated by scanning electron microscopy (FEG-SEM) and atomic force microscopy (AFM). SEM micrographs were obtained by using a Tescan Mira III. Samples (15 mm  $\times$  1 mm  $\times$  1 mm) were cryofractured and sputter-coated with gold before imaging. The dynamic tapping mode of an AFM (Nanotec) was used to obtain simultaneous micrographs of the topography and oscillatory phase of different Pus scanning at room temperature. The amplitude setpoint was adjusted at

65% of the free amplitude value to set the tip-sample interaction in the moderate force range. Under these conditions, phase data are sensitive to differences in the local stiffness of the PU domains.

The CE effect on the crystallinity and size domains were evaluated by wide-angle X-ray diffraction (WAXD) and small-angle X-ray scattering (SAXS). WAXD was performed in a Shimadzu XRD-6000 diffractometer operating in reflection mode using  $\text{Cu K}\alpha$  radiation ( $\lambda = 1.5405 \text{ \AA}$ ). Data were collected over  $2\theta$  angles ranging from  $1^\circ$  to  $40^\circ$  at  $0.5^\circ/\text{min}$  scanning rate. SAXS experiments were performed on the SAXS1 beamline of the Brazilian Synchrotron Light Laboratory (LNLS), monitored with a photomultiplier, and detected on a Pilatus (300 k, 84 mm  $\times$  107 mm) positioned at 836 mm. The generated scattering wave vectors ( $q$ ) ranged from  $0.13$  to  $2.5 \text{ nm}^{-1}$  at room temperature. The wavelength of the incident X-ray beam ( $\lambda$ ) was  $0.155 \text{ nm}$ . Samples with 3 mm in diameter and 0.5 mm thick were used. A silver behenate ( $\text{AgBeH}$ ) standard was used for calibrating the diffracting angle. The background and parasitic scattering were determined in separate measurements on an empty holder and subtracted from the sample scattering.

### 3 | RESULTS AND DISCUSSION

The synthesized PUs showed the gelled structures formation due to the average functionality of the polyol used. The GC for all PUs regardless of the CE type used was  $\sim 85\%$ . PUs FTIR spectra after the polymerization procedure are shown in Figure 1. After 96 h of the

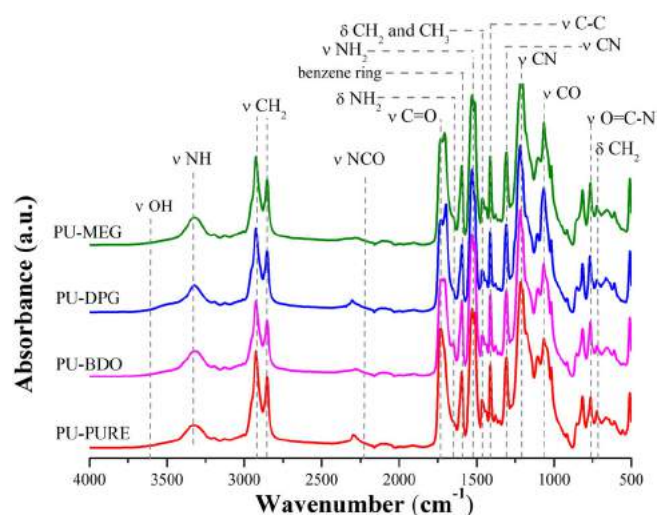


FIGURE 1 Fourier transform infrared spectra of polyurethane (PU) with chain extenders (CEs) as: PU-MEG, PU-BDO, and PU-DPG and PU-PURE (without CE) [Color figure can be viewed at [wileyonlinelibrary.com](http://wileyonlinelibrary.com)]



polymerization reaction, the characteristic hydroxyl of the polyol ( $-\text{OH}$ ) at  $3600\text{--}3300\text{ cm}^{-1}$  and isocyanate ( $-\text{NCO}$ ) at  $2277\text{ cm}^{-1}$  bands disappeared completely for all PUs (PU-PURE, PU-BDO, PU-MEG, and PU-DPG). Subsequent complete polymerization characteristic bands of the urethane group formation and triglyceride bands were observed in all PUs.<sup>9,10</sup> The band at  $1735\text{ cm}^{-1}$  is assigned to the stretching mode of the carbonyl ester group ( $\text{C}=\text{O}$ ) of the soybean oil. Aliphatic hydrocarbons groups in the soft domain (from SOP and CEs) are visible at  $1463$ ,  $2922$ , and  $2855\text{ cm}^{-1}$ , while bending vibrations of the  $-\text{CH}_2$  appear at  $722\text{ cm}^{-1}$ ,<sup>13,18</sup> and double bonds ( $[\text{C}=\text{C}]-\text{H}$ ) peak at  $3010$  and  $1640\text{ cm}^{-1}$ .<sup>10,11</sup> The band at  $1217\text{ cm}^{-1}$  corresponds to the stretching mode of the carbonyl ester ( $\text{CO}-\text{O}$ ) in the single bond configuration ( $\text{C}-\text{O}$ ), arising most probably from glycerol groups ( $\text{COH}$ ).<sup>12,13</sup> The consecutive bands at  $1307$ ,  $1500$ , and  $1520\text{ cm}^{-1}$  are attributed to stretching modes of  $\text{CN}$ ,  $\text{CH}_2-\text{CH}_3$ , and  $\text{NH}_2$ .<sup>14</sup> The band at  $3318\text{ cm}^{-1}$  is assigned to the free  $\text{N}-\text{H}$  stretching vibration of the urethane groups, while the urea groups formation is evidenced through the stretching mode ( $-\text{NH}_2$ ) at  $1654\text{ cm}^{-1}$  and the benzene ring domain in MDI (band at  $1600\text{ cm}^{-1}$ ).<sup>15</sup>

The hydrogen bond amount and distribution contribute to the phase separation degree in PU materials.<sup>5</sup> The main band that contributes to the inter-urethane hydrogen bonds formation shows up in the carbonyl region ( $1600\text{--}1800\text{ cm}^{-1}$ ).<sup>16-18</sup> These bands have been found useful for the relative amount determination of hydrogen bonds in petrochemical polyols, for example, carbonate-based polyol.<sup>1,17</sup> However, for renewable polyols such as SOP, this kind of study is not yet available in the literature. The FTIR spectra mathematical deconvolution can be used to understand the phase separation. For this approach, three contributions were attributed to SOP carbonyl band: band  $\text{I}_{\text{SOP}}$  at  $1742\text{ cm}^{-1}$ , assigned to free carbonyl groups unbounded hydrogen bonds; band  $\text{II}_{\text{SOP}}$  at  $1720\text{ cm}^{-1}$ , identified as physically bounded carbonyl groups by dipole-dipole interactions; and band  $\text{III}_{\text{SOP}}$  at  $1700\text{ cm}^{-1}$ , ascribed to physically bonded carbonyl group by hydrogen bonding interactions (between SOP  $-\text{OH}$  end groups and  $\text{C}=\text{O}$  groups of the urea bond).

To confirm the bands' assignment, according to the method proposed by Niemczyk,<sup>17</sup> the SOP was analyzed for 24 h under the following conditions: dry, immersed in water ( $\text{H}_2\text{O}$ ), and immersed in ammonia solution ( $\text{NH}_4\text{OH}$ ). Each band area was analyzed through the mathematical deconvolution of the FTIR, which is shown in Table 1. FTIR spectra deconvolution results of the pure polyol are shown in the supporting information (Figure S1). After immersion of the SOP in  $\text{H}_2\text{O}$  bands,  $\text{I}_{\text{SOP}}$  and  $\text{III}_{\text{SOP}}$  were observed to decrease. This indicates that water molecules did not form new hydrogen bonds.

Meanwhile, the area of the  $\text{II}_{\text{SOP}}$  band increases. This behavior indicates an increased interaction between the hydroxyl group ( $-\text{OH}$ ) and the urea bond ( $\text{C}=\text{O}$ ) by SOP physically bounded hydrogen bonds. As expected, after immersion in  $\text{NH}_4\text{OH}$ , the SOP formed new hydrogen bonds between the  $\text{N}-\text{H}$  (from  $\text{NH}_4\text{OH}$ ) and  $\text{C}=\text{O}$  (from SOP), as evidenced by the intensity increase of  $\text{II}_{\text{S.O.P}}$  bands and the formation of a new band at  $1675\text{ cm}^{-1}$  labeled as  $\text{IV}_{\text{S.O.P}}$ . The new band confirms that carbonyl groups that undergo hydrogen interactions are competitive bonds, which may interact with the hydroxyl or amine groups.<sup>17</sup>

FTIR spectra and its deconvolution are shown in Figure 2(a) for all PUs in the carbonyl region (PU-PURE, PU-BDO, PU-DPG, and PU-MEG). In the case of the PUs obtained with CEs, PU-BDO, PU-MEG, and PU-DPG, we observed the displacement to lower wavenumber of the carbonyl group stretching vibration related to polyol. It is an assignment to the urethane carbonyl bonding formation associated with the hard domain organization.<sup>11</sup> FTIR deconvoluted spectra of PUs treated with CEs are shown in Figure 2(b-d) (PU-BDO), (PU-DPG), and (PU-MEG). The FTIR spectrum in the carbonyl region corresponding to PU-PURE deconvoluted in six bands (showed in the supporting information [Figure S2]). The six bands are assigned as follows: (I) at  $1643\text{--}1650\text{ cm}^{-1}$  H-bonded urethane carbonyl groups appear (ordered phase-hard domain); (II) the band at  $1660\text{--}1675\text{ cm}^{-1}$  corresponds to H-bonded urethane carbonyl groups (disordered phase-hard domain); (III) H-bonded carbonyl groups (soft-hard domain) are observed at  $1690\text{ cm}^{-1}$ ;

**TABLE 1** Values of peak position and areas in the carbonyl region of the soybean oil polyol (SOP) by Fourier transform infrared spectroscopy

Samples	Band $\text{I}_{\text{S.O.P}}$		Band $\text{II}_{\text{S.O.P}}$		Band $\text{III}_{\text{S.O.P}}$		Band $\text{IV}_{\text{S.O.P}}$	
	Peak center ( $\text{cm}^{-1}$ )	Area (%)	Peak center ( $\text{cm}^{-1}$ )	Area (%)	Peak center ( $\text{cm}^{-1}$ )	Area (%)	Peak center ( $\text{cm}^{-1}$ )	Area (%)
S.O.P - pure	1742	$75.6 \pm 0.1$	1720	$20.1 \pm 0.1$	1699	$4.3 \pm 0.0$	—	—
S.O.P - $\text{H}_2\text{O}$	1742	$73.6 \pm 0.1$	1721	$22.2 \pm 0.1$	1700	$4.2 \pm 0.0$	—	—
S.O.P - $\text{NH}_4\text{OH}$	1742	$71.0 \pm 0.6$	1722	$21.3 \pm 0.4$	1700	$5.4 \pm 0.2$	1675	$2.2 \pm 0.3$

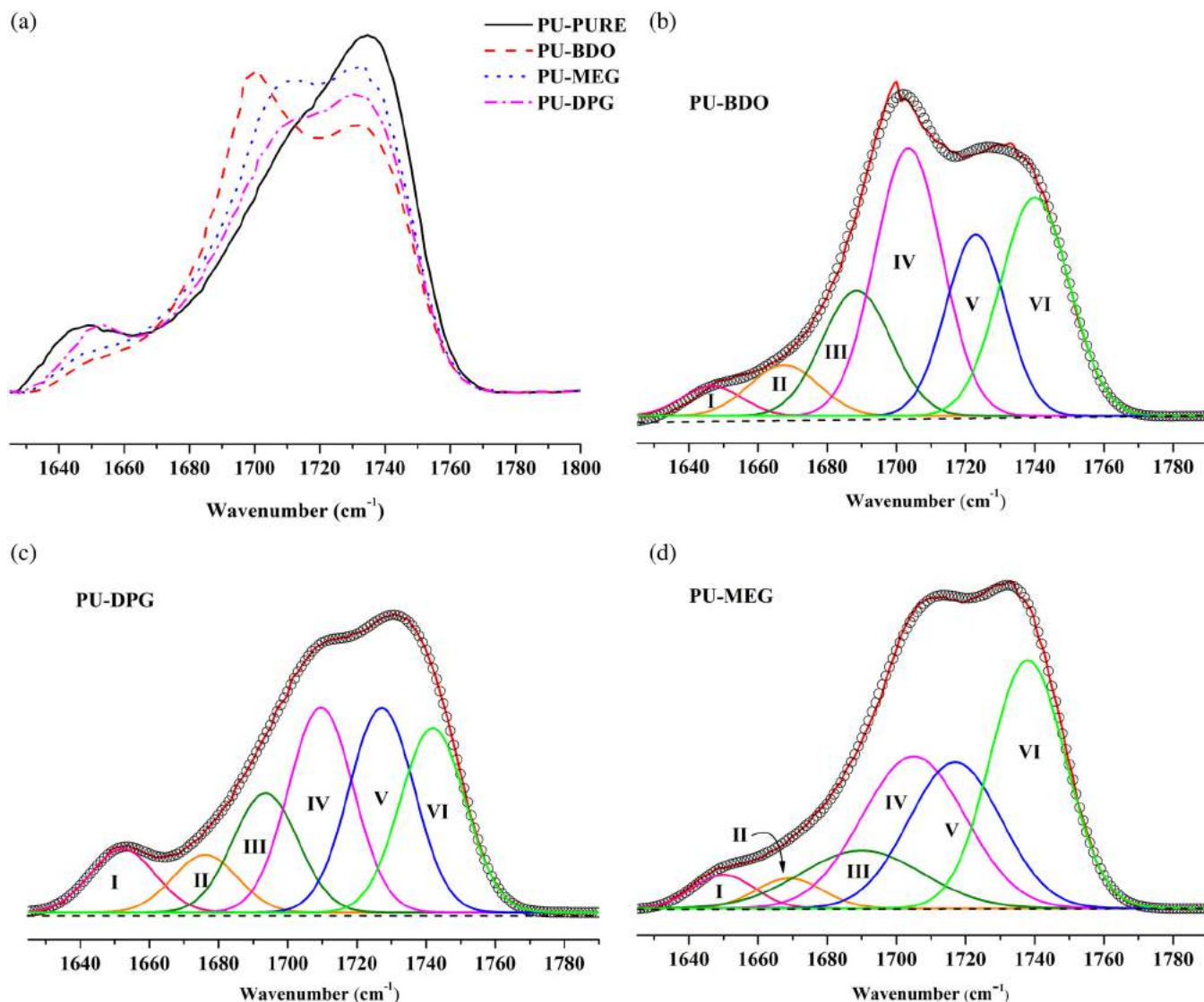


FIGURE 2 Fourier transform infrared PUs spectra: (a) N–H absorbance and the carbonyl absorbance regions and deconvolution spectra in the region carbonyl group for PUs with chain extenders (CEs); (b) PU-BDO, (c) PU-DPG, and (d) PU-MEG [Color figure can be viewed at [wileyonlinelibrary.com](http://wileyonlinelibrary.com)]

(IV) at  $1703\text{--}1707\text{ cm}^{-1}$  urethane free carbonyl group (hard domain) appear; (V) at  $1717\text{ cm}^{-1}$  we observe carbonyl groups (soft domain) associated to SOP; (VI) finally, at  $1740\text{ cm}^{-1}$  there are free carbonyl groups (soft domain) associated to SOP. The weight fraction of hydrogen-bonded urethane groups ( $X_b$ ) as well as of the hard domain dispersed soft domain ( $W_h$ ), evaluated with Equations ((3) and ((4), are shown in Table 2.

$$X_b = \frac{A_b}{k'A_b + A_f} = \frac{A_{1643-1650} + A_{1660-1675}}{k'A_{1703-1707} + A_{1643-1650} + A_{1660-1675}} \quad (3)$$

$$W_h = \frac{(1-X_b)f}{[(1-X_b)f + (1-f)]} \quad (4)$$

where  $A_b$  is the area associated H-bonds between two urethane groups (bands I and II),  $A_f$  is the absorbance of urethane free carbonyl group (band IV),  $k'$  is a constant equal 1.2 (extinction coefficient),<sup>16</sup> and  $f$  is the hard domain weight fraction in the polymer from initial molar ratios. The mixed-phase weight fraction (MP), the soft phase weight fraction (SP), and the hard phase weight fraction (HP) were computed according to the Equations (5), (6), and (7)<sup>1,17</sup>:

$$MP = fW_2' \quad (5)$$

$$SP = MP + (1-f) \quad (6)$$

$$HP = 1 - SP \quad (7)$$

To be able to estimate  $X_b$ ,  $W_h$ ,  $MP$ ,  $SP$ , and  $HP$ , we assumed that hydrogen bonds are only present on the hard domain.<sup>1,17</sup> To confirm the assumptions, we use the Fox equation.<sup>19</sup> The Fox equation is described as:  $1/T_{gs} = (1 - W_{h,Fox})/T_{gs^0} + W_{h,Fox}/T_{gH^0}$ , where,  $T_{gH^0}$  is the hard domain glass transition, thus for MDI/BDO,  $T_{gH^0} = 110^\circ\text{C}$ , MDI/MEG  $T_{gH^0} = 139^\circ\text{C}$  and MDI/DPG  $T_{gH^0} = 108^\circ\text{C}$ .<sup>2,20,21</sup> The  $T_{gs^0}$  is the temperature corresponding to the soft domain glass transition, with the SOP  $T_{gs^0} = -80^\circ\text{C}$ . The  $T_{gs^0}$  and  $T_{gH^0}$  values were determined by DMA and DRS analysis. The  $W_h$  value was comprised between 0.2 and 0.35 for all PUs (Table 2).

The  $MP$  value increased for PUs with CEs (PU-MEG, PU-BDO, and PU-DPG). As expected, the amount of mixed-phase without the CE addition should tend to the lowest possible value, as there is no contribution from CEs to the organized domain formation. There is a relative increase in the density of hydrogen bonds in PUs with CEs due to the greater regularity in the chain to form interactions. Thus, the value of  $X_b$  increases with the CE addition. Overall, soybean PU synthesized with polyols with functionality greater than 2, do not tend to form organized structures.<sup>7,22</sup> An interesting effect was observed for  $MP$  values. As CEs were added, the degree of phase-mixed increased, which is a commonly not observed effect on PUs since the CEs addition tends to contribute to the organized hard domains formation, which results in the creation of the supramolecular structures. Concerning the  $SP$  and  $HP$  fractions, there were not practically differences in the values obtained without and with CE, regardless of the nature of the latter.

The miscibility degree between the hard and soft domains depends strongly on the chemical composition formed in each domain. This trend increases according to the interaction between the hard and soft domains and, also with the content of the hard domains generated when some of them are dissolved in the soft phase.<sup>23</sup> The monomers' solubility parameters ( $\delta$ ) were calculated according to Van Krevelen.<sup>24</sup> The soft domain, SOP composed, showed  $\delta = 24.86 \text{ J}^{1/2}/\text{cm}^{1/2}$ . Meanwhile, in the hard domain, the miscibility degree decreased in the following order: MDI – DPG > MDI – BDO > MDI – MEG with  $\delta = 24.89, 25.41, \text{ and } 26.54 \text{ J}^{1/2}/\text{cm}^{1/2}$ , respectively. Although, there is a tendency for hydrogen bond density to increase by the CEs addition, the hard

phase formation effect, as traditionally noted in PUs, is suppressed by the functionality of the polyol and mixed-phase amount. Thus, the best mechanical, thermal, and hydrolysis resistance properties will depend strongly on the chemical structure, shape, and distribution of the hard domains, since in the mixed-phase region, there is higher entropy when compared to an organized structure hard domain.<sup>5,15</sup>

Figure 3 shows the DSC thermograms of the PU-PURE, PU-MEG, PU-BDO, and, PU-DPG. All PUs showed the Schatzki mechanism at  $-111^\circ\text{C}$  associated with the group  $-\text{CH}_2-$  rotation motion in the amorphous region.<sup>25</sup> It is typical of hydrocarbon-based polymers.<sup>25</sup> At low temperatures, the fatty acids melting peak disappeared, showing a broad transition peak when compared to pure polyol.<sup>4</sup> After polymerization, a fraction of fatty acids loses mobility due to the formation of hydroxyl groups and reaction to form urethane. The PUs had a fusion endotherm comprised between  $40$  and  $70^\circ\text{C}$ , which may be associated with a hard-domain glass transition temperature ( $T_{gH}$ ). On the other hand,  $\alpha$ -transitions are found at temperatures slightly lower than  $T_{gH}$ .<sup>26</sup> However, the PU molecular motions involved near the soft-domain glass transition temperature ( $T_{gS}$ ) and  $T_{gH}$ , cannot be accurately obtained by DSC analysis due to the broad peak fusions of the soybean oil. In this way, it became necessary to use complementary analyzes such

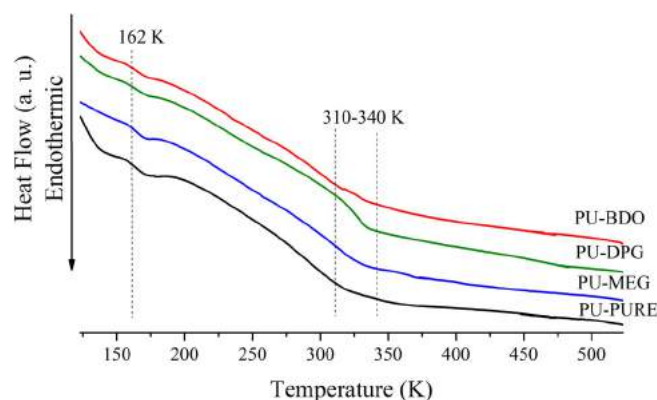


**FIGURE 3** Differential scanning calorimetry thermograms of PU-PURE (without chain extender [CE]) and PU with different CEs: PU-MEG, PU-BDO and PU-DPG [Color figure can be viewed at [wileyonlinelibrary.com](http://wileyonlinelibrary.com)]

**TABLE 2** Parameters for phase separation degree determination in soybean polyurethanes (PUs)

	$X_b$	$W_h$	MP	SP	HP
PU-PURE	$0.21 \pm 0.15$	$0.26 \pm 0.05$	$0.08 \pm 0.00$	$0.77 \pm 0.01$	$0.23 \pm 0.01$
PU-BDO	$0.29 \pm 0.01$	$0.31 \pm 0.00$	$0.12 \pm 0.01$	$0.73 \pm 0.01$	$0.27 \pm 0.01$
PU-MEG	$0.30 \pm 0.02$	$0.31 \pm 0.01$	$0.12 \pm 0.01$	$0.73 \pm 0.01$	$0.27 \pm 0.01$
PU-DPG	$0.27 \pm 0.03$	$0.33 \pm 0.01$	$0.13 \pm 0.00$	$0.73 \pm 0.01$	$0.27 \pm 0.01$

as DMA and DRS. These give an unmistakable reading of the maximum peaks' position.<sup>2,27,28</sup>

The macromolecular motions involved in  $T_{gH}$ ,  $T_{gS}$ , and Schatzki mechanism for PU-PURE, PU-BDO, PU-MEG, and PU-DPG were obtained from the peaks of the  $\tan \delta$  curves by DMA and DRS. The corresponding spectra AR 1 Hz are shown in Figure 4. The results confirm the trends seen in DSC analysis for the Schatzki mechanism at  $-111^\circ\text{C}$ . The low temperature the PU-PURE showed a  $T_{gS}$  around  $-35^\circ\text{C}$ . The PUs with CEs (PU-BDO, PU-MEG, and PU-DPG) showed a  $T_{gS}$  around  $-21^\circ\text{C}$ , while SOP had a  $-80^\circ\text{C}$   $T_g$ .<sup>4</sup> Thus, for all PUs the  $T_{gS}$  increase. It indicates that there was a mixing degree between the hard and soft domain and in the phase-mixed, as expected. The CEs produced a pronounced effect on the PUs  $T_{gH}$ . The high-temperature transition,  $T_{gH}$ , increased in the following order: PU-PURE < PU-MEG < PU-BDO < PU-DPG. The  $T_{gH}$  decreases systematically with increasing CEs methylene sequences lengths ( $-\text{CH}_2-$ ).<sup>29</sup> The PU-BDO and PU-MEG follow this trend, while the PU-DPG does not follow this same behavior due to the oxygen atom (heteroatom) present in the polymer chain. In the literature,<sup>2</sup> it was found for soybean PUs, that the  $T_{gH}$  behavior strongly depends on the molecular weight and the hard domain amount formed. Corcuera et al.<sup>30</sup> synthesized castor PUs with different amounts of the hard domain, using MDI and BDO as CE. The authors observed that a more substantial hard domain amount the  $T_g$  tends to increase due to a higher crosslink density. Castor PUs with 20–50 wt% hard domain presented a  $T_{gS}$  from  $-45$  to  $-20^\circ\text{C}$  and  $T_{gH}$  from 47 to  $62^\circ\text{C}$ . The results obtained so far are in agreement with the literature for PUs based on vegetable oils.<sup>17,31,32</sup>

The temperature dependence on the storage modulus ( $E'$ ) for PU-PURE, PU-MEG, PU-BDO, and PU-DPG by DMA are shown in Figure 5. In the vitreous region, the modulus in all PUs starts from values  $>10^9$  Pa, following the expected trends (solid-like behavior). The PU-BDO and PU-DPG had relative rigidity because they present higher  $E'$ . It gives rise to a high crosslinking physical density due to the increased phase separation degree when compared to PU without CEs (PU-PURE).<sup>33,34</sup>

Figure 6 shows the temperature and frequency ( $\omega = 2\pi f$ ) dependence on the complex dielectric permittivity,  $\epsilon^*(\omega) = \epsilon'(\omega) - i\epsilon''(\omega)$ , for PU-PURE, PU-MEG, PU-BDO, and PU-DPG samples. In general, dielectric relaxation modes are consistent with DSC and DMA results. For all PUs, the spectra are complicated presenting processes of a different nature, dipole, and conductive, in some cases closely superimposed. The soybean PUs mobility is dependent on the type of CE chosen for PU synthesis, which directly influences the hard domains formed amount. For the CE, the greater the  $-\text{CH}_2-$  groups sequence in the main chain, the thermal transitions are also modified. At temperatures below  $-30^\circ\text{C}$ , the dielectric constant ( $\epsilon'$ ) shows values that vary only slightly with frequency. Its contribution is originated from the electronic polarization of small groups induced by the electric field.<sup>24</sup> The rapid increase in  $\epsilon'$  between  $-30^\circ\text{C}$  and  $40$ – $50^\circ\text{C}$  reveals the amorphous unfreezing soft domains component. Finally, the strong increase in the dielectric constant values for temperatures above  $50^\circ\text{C}$  is associated with the hard glass transition and with the presence accumulation of charges at the electrode-sample interface, referred to as “electrode polarization” (EP).<sup>22,35</sup>

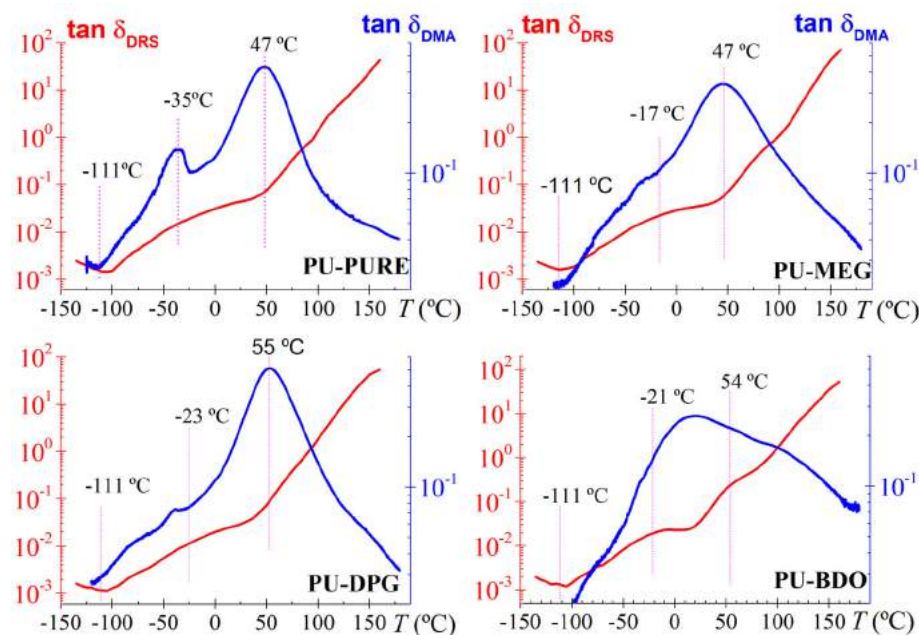


FIGURE 4 Tan  $\delta$  versus temperature at 1 Hz of PU-PURE and PU with different chain extenders (CEs): PU-MEG, PU-BDO, and PU-DPG [Color figure can be viewed at [wileyonlinelibrary.com](http://wileyonlinelibrary.com)]



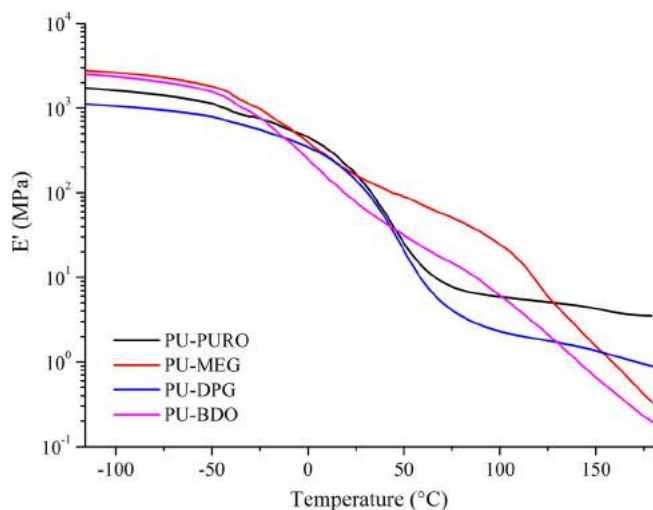


FIGURE 5 Storage modulus-temperature curves of (a) PU-PURE (without chain extender [CE]) and PU with different CEs: (b) PU-MEG, (c) PU-BDO, and (d) PU-DPG [Color figure can be viewed at [wileyonlinelibrary.com](http://wileyonlinelibrary.com)]

For all PUs, the loss factor ( $\epsilon''$ ) spectra show two secondary processes, around  $-21^\circ\text{C}$  ( $\beta$ -transition) and  $-69^\circ\text{C}$  ( $\gamma$ -transition). The last transition labeled as the Schatzki mechanism is related to the short group rotation in the fatty acid chains.<sup>36</sup> These short segment motions are observed in most hydrocarbon polymers.<sup>4</sup> At higher temperature, the increase of the loss permittivity is associated with the glass transition temperature of the soft and hard domains of the PU, which are closely overlapped with different nature conductive processes (ionic conductivity and interfacial polarization effects originated from the charges accumulation at the electrode-polymer interface) are especially dominant at high temperatures and low frequencies.<sup>35</sup> The glass transition of the soft domains is associated with the carbonate groups motions, whereas hard isocyanate segments glass transition (hard domain)<sup>36</sup> is linked to the CEs after polymerization. These charges can be associated as arising from side chains motions change the orientation of the ether group dipole moment. Conductivity processes are associated with the migration of mobile charge carriers through the medium and with charges trapped at interfaces and boundaries. Thus, its additional polarization is the (a) charges accumulation result at the electrode-sample interface called “electrode polarization” (EP)<sup>22,35</sup> and/or (b) the charges separation at internal phase boundaries referred to as Maxwell-Wagner-Sillars (MWS) polarization.<sup>37–39</sup> The last conductive processes have been evidenced in other PU systems.<sup>38,40</sup>

To characterize the low-temperature relaxation process (the Schatzki dipolar process,<sup>41</sup> also labeled as  $\gamma$ -process), the Havriliak-Negami (HN) empirical model, was

employed. For each sample, the four HN fitting parameters ( $\Delta\epsilon$ ,  $a$ ,  $b$  and  $\tau$ ) were determined, at several temperatures, from a multiple nonlinear regression analysis of the experimental isotherms of loss permittivity ( $\epsilon''$ ).

The strength relaxation ( $\Delta\epsilon = \epsilon_0 - \epsilon_\infty$ ), that is the difference between the relaxed ( $\epsilon_0$ , the dielectric constants on the low frequency/long times) and unrelaxed permittivity ( $\epsilon_\infty$ , the dielectric constant on the high frequency/short times), is related to both the concentration and the dipole moment of the dipolar entities implied in the process, taking into account the possible orientational correlation between dipoles.<sup>7,8</sup> The shape parameters,  $a$  and  $b$ , are related to the distribution and symmetry of the relaxation and  $\tau$  represents the relaxation time of the process.

The temperature dependence on the dielectric strength ( $\Delta\epsilon$ ) of the  $\gamma$ -transition between  $-133$  to  $-93^\circ\text{C}$  for PU-PURE, PU-MEG, PU-BDO, and PU-DPG is shown in Figure 7(a). As previously indicated, the  $\Delta\epsilon$  is related to the mobile dipoles fraction involved in the relaxation process, which could reflect the molecular interaction in the phase separation degree.<sup>37</sup> In all PUs, the value of  $\Delta\epsilon$  increases slightly with increasing temperature due to the dipoles' mobility, connected mainly with the free volume increase. This behavior is consistent with the thermally activated mechanism, following PUs classical trends.<sup>38</sup> Concerning PU-PURE, while an increase in  $\Delta\epsilon$  is observed for PU-MEG, a reduction is observed for the PU-BDO and PU-DPG samples. Thus, the PU-MEG showed higher mobility with  $\Delta\epsilon = 0.110$ , and PU-BDO and PU-DPG had less mobility with  $\Delta\epsilon = 0.08$ . This mobility loss is attributed to the increase in the crosslinking degree during PU synthesis. This happened because of the greater distance between the CEs hydrogen bonds. Besides that, when the shape parameter ( $a$ ) is evaluated in all PUs with CEs (in Figure 7(b)), the results are in agreement with the data obtained in  $\Delta\epsilon$ . For all PUs, the  $\gamma$ -transition presented is a very distributed load character due to the low value of 0.23–0.3.<sup>42</sup> In all the samples, the shape parameter  $b$  was equal to unity for all the temperatures analyzed, indicating the analyzed relaxation process symmetry. The greater the decreases, generating methylene groups sequence ( $-\text{CH}_2-$ ) of the CE in the soybean PU, the process amplitude in  $a$  is slightly less mobility to PU. Thus, highlighting that the PU-BDO after the polymerization and curing process presented itself as an extremely hard film. The PU-DPG film, for having oxygen in its structure (heteroatom), was a slightly malleable material. While PU-MEG presented itself as an extremely flexible and resistant film. Velayutham et al.<sup>34</sup> evaluated the chemical contribution effect on the PUs dielectric behavior. In this work, the authors synthesized PUs from palm/TDI/oleic acid ( $[\text{NCO}]/[\text{OH}] = 1.1/1.0$  mol/mol molar ratio). They evidenced that PUs mobility was reduced due to the increase in relaxation time, which is proportional to the

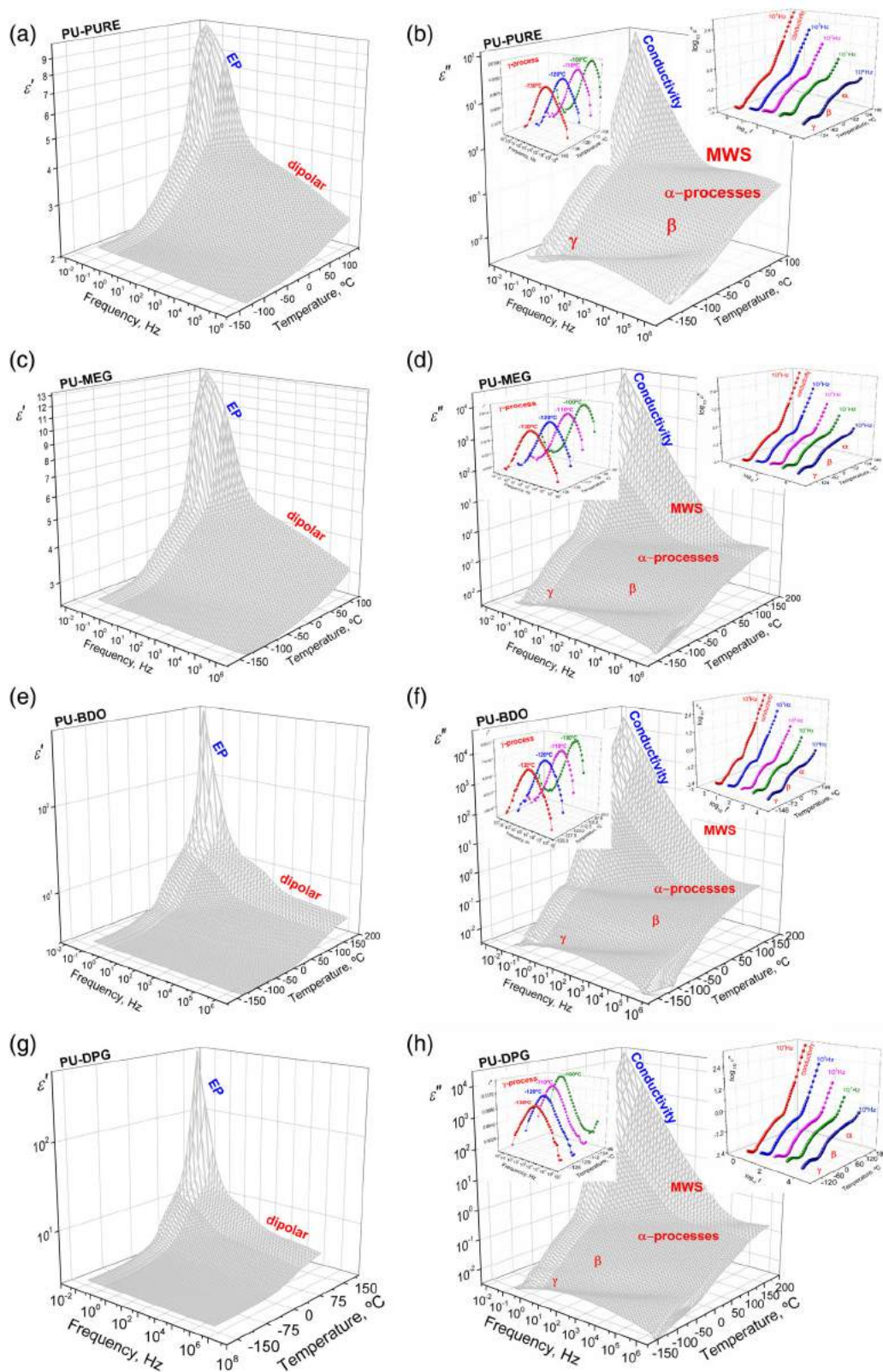


FIGURE 6 3D representation of the dielectric permittivity of PU-PURE, PU-MEG, PU-BDO, and PU-DPG [Color figure can be viewed at [wileyonlinelibrary.com](http://wileyonlinelibrary.com)]

increase in the crosslinks degree. Finally, Figure 7(c) shows the temperature dependence on the relaxation time ( $\ln \tau$ ) of the  $\gamma$ -transition for PU-PURE, PU-MEG, PU-BDO, and PU-

DPG samples. Thus, the  $\gamma$ -transition is thermally activated, exhibiting Arrhenius behavior (ARRH).<sup>36</sup> The ARRH parameters, the activation energies ( $E_a$ ), and pre-exponential

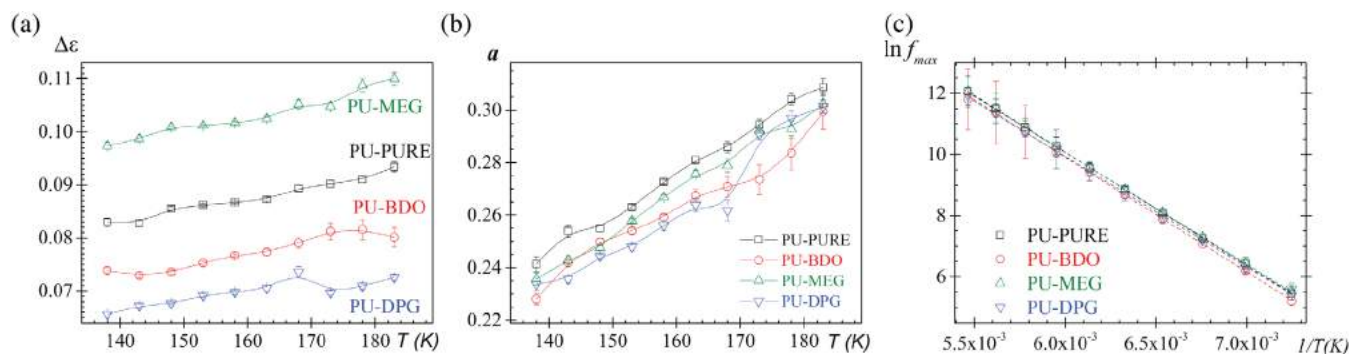
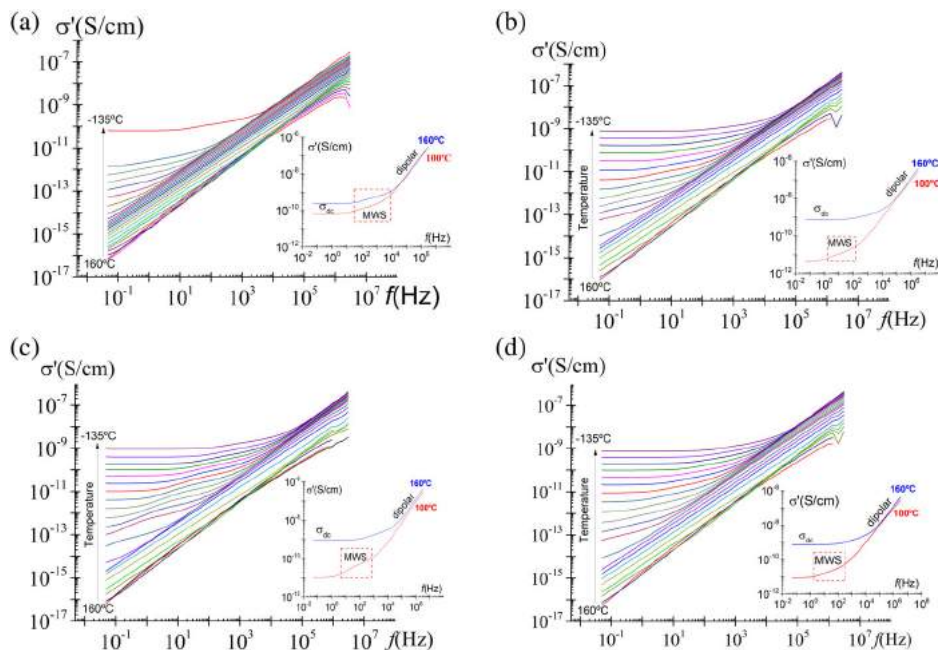


FIGURE 7 Temperature dependence on: (a) dielectric strengths ( $\Delta\epsilon$ ), (b)  $a$  shape parameter, and (c)  $\ln f_{max}$ , of Schatzki process for PU-PURE, PU-MEG, PU-BDO, and PU-DPG [Color figure can be viewed at wileyonlinelibrary.com]

TABLE 3 Arrhenius fit parameters of the  $\gamma$ -transition (Schatzki process): Activation energy ( $E_a^\gamma$ ), and pre-exponential factors ( $\tau_0 = 2\pi f_{max}$ ) and activation energy ( $E_a^\sigma$ ) for PU-PURE, PU-BDO, PU-MEG, and PU-DPG

	PU-PURE	PU-MEG	PU-BDO	PU-DPG
$E_a^\gamma$ , kJ/mol	$30.80 \pm 0.13$	$30.42 \pm 0.06$	$31.20 \pm 0.11$	$30.02 \pm 0.37$
$\tau_0$ , s	$10^{-14.83} \pm 10^{-0.84}$	$10^{-14.71} \pm 10^{-0.82}$	$10^{-14.88} \pm 10^{-0.84}$	$10^{-14.52} \pm 10^{-0.93}$
$E_a^\sigma$ , kJ/mol	$96.04 \pm 0.29$	$116.74 \pm 0.65$	$99.03 \pm 1.11$	$102.33 \pm 0.89$

FIGURE 8 Frequency dependence on the real conductivity for (a) PU-PURE (without chain extender [CE]), (b) PU-MEG, (c) PU-BDO, and (d) PU-DPG at several temperatures (from  $-130$  to  $160^\circ\text{C}$ , step  $10^\circ\text{C}$ ) [Color figure can be viewed at wileyonlinelibrary.com]



factors ( $\tau_0$ ) for PU-PURE, PU-MEG, PU-BDO, and PU-DPG are given in Table 3. In all PUs, the  $E_a$  values are similar around  $30.6$  kJ/mol, agreeing with the results found in the literature for  $\gamma$ -transition in PUs from vegetable oils.<sup>43</sup>

Unfortunately, the  $\beta$ -dipolar relaxation process characterization is prevented by the close overlap that exists between them and the relaxation process associated with the soft domains glass transition. In the same way, the last ones highly overlapped with the relaxation process associated with the glass transition of the PUs hard domains, and these with the MWS process. To

characterize the conductive process that dominates the dielectric spectra low frequencies and high temperatures, the complex ac conductivity  $\sigma_{ac}^*(\omega) = \sigma'(\omega) + i\sigma''(\omega)$  was evaluated from the complex dielectric permittivity  $\epsilon^*$  according to  $\sigma^*(\omega) = i\omega\epsilon_0\epsilon^*(\omega)$ , where  $\epsilon_0$  is the vacuum permittivity. So, the real part of  $\sigma^*(\omega)$  is given by  $\sigma'(\omega) = \sigma'_{ac}(\omega) = \omega\epsilon_0\epsilon''(\omega)$ . As usual in the frequency domain, the isotherms corresponding to high temperatures exhibit a plateau in the low-frequency region, reflecting a frequency-independent conductivity, that is, dc conductivity. The PUs bulk conductivity increases



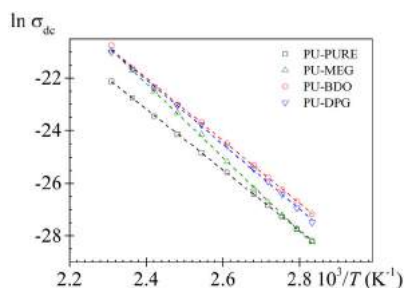


FIGURE 9 Temperature dependence on the dc conductivity (s/cm) for PU-PURE (without chain extender [CE]), PU-MEG, PU-BDO, and PU-DPG [Color figure can be viewed at [wileyonlinelibrary.com](http://wileyonlinelibrary.com)]

with increasing frequency, as expected for an insulator material. The last tendency is amorphous polymers characteristic and is related to phenomena such as whole translational molecules, cooperative jumps, disorientations, and chain segments relaxations.<sup>44</sup> Between the dc conductivity and the linear increase in conductivity at high frequencies, it is observed MWS relaxation creates a “knee”-like an increase of the  $\sigma$  curve in the middle part of the isotherm, which is uniformly shifted with temperature. As indicated above, the MWS process<sup>36,43,45</sup> is related to the build-up of charges at the interfaces of the microphase separation of the soft and hard domains. Figure 9 shows the dc conductivity values

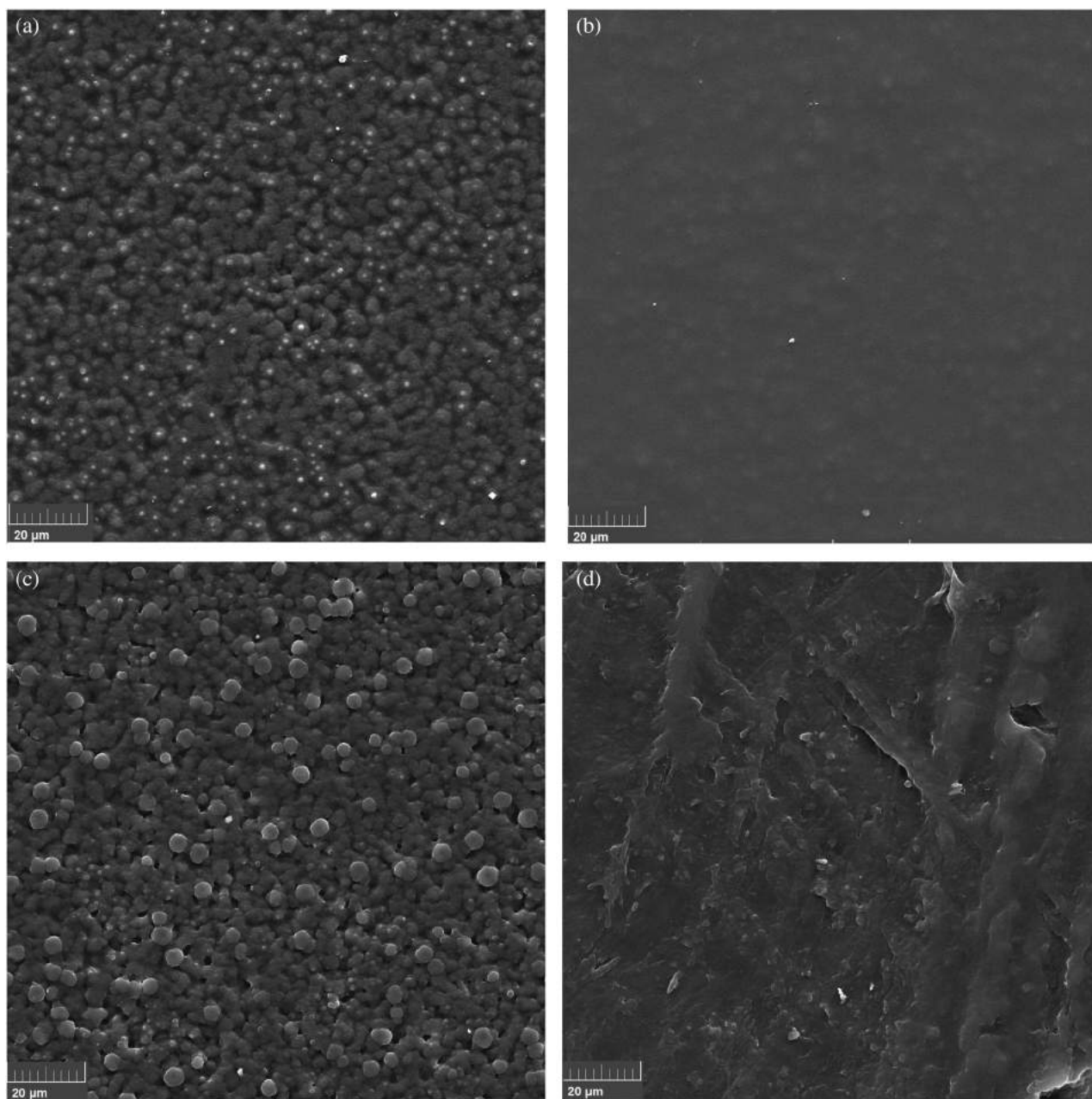


FIGURE 10 FEG-SEM surface micrographs of PUs: (a) PU-PURE (without chain extender [CE]), (b) PU-DPG, (c) PU-MEG, and (d) PU-BDO



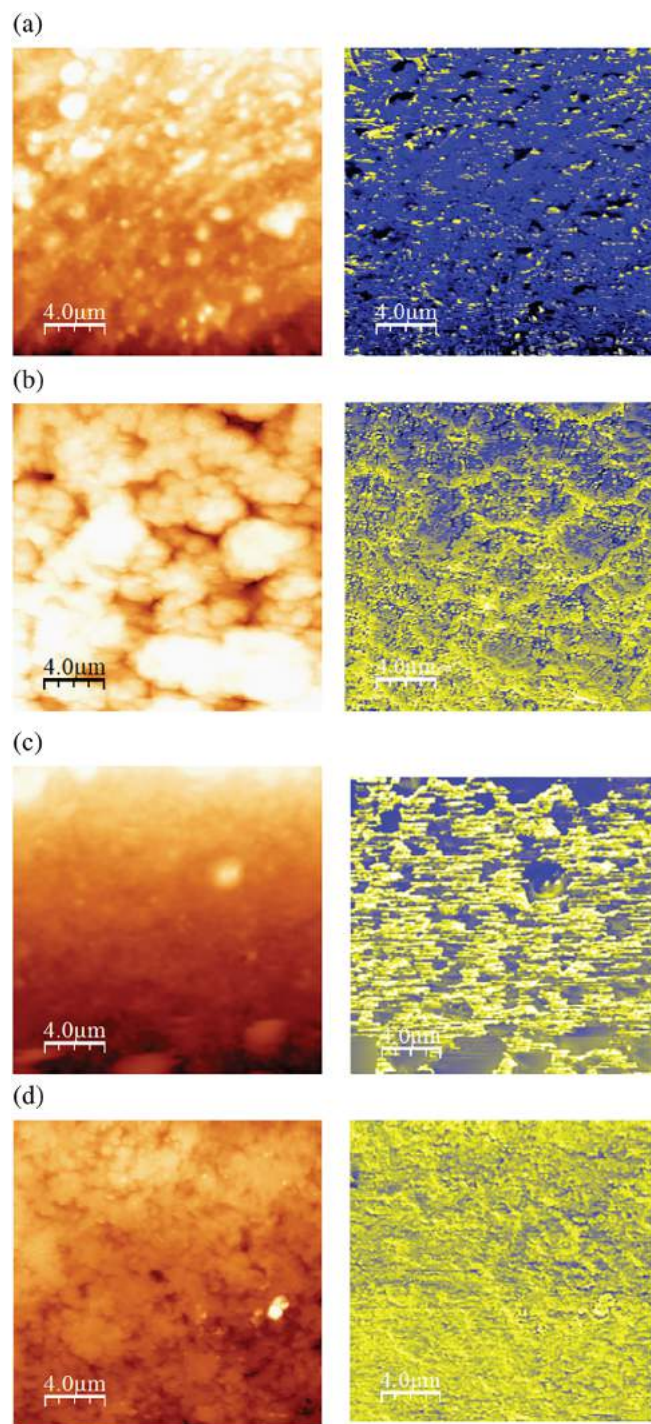


FIGURE 11 Height (left) and oscillatory phase (right) AFM images of (a) PU-PURE (without chain extender [CE]), (b) PU-DPG, (c) PU-MEG, (d) PU-BDO [Color figure can be viewed at [wileyonlinelibrary.com](http://wileyonlinelibrary.com)]

obtained at several temperatures from extrapolations to low frequencies as a reciprocal temperatures function obeys an Arrhenius behavior with activation energy values given in Table 3.

Figure 10 shows the SEM surface micrographs for the PU-PURE, PU-DPG, PU-MEG, and PU-BDO. All PUs

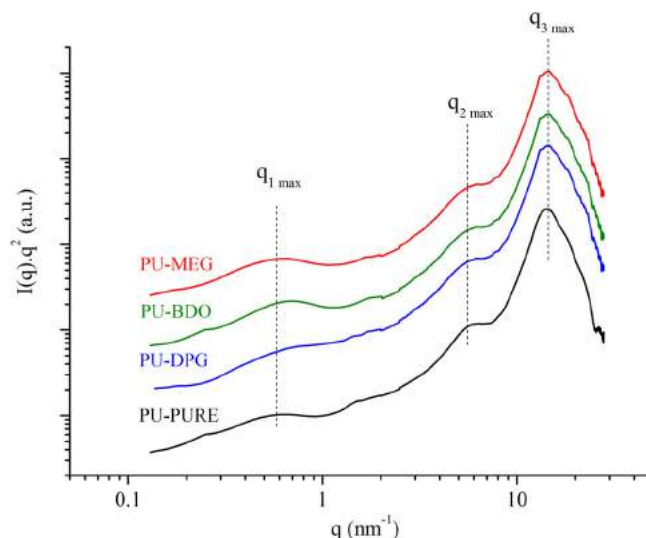


FIGURE 12 SAXS-WAXD patterns of PU: PU-PURE, PU-DPG, PU-MEG, and PU-BDO [Color figure can be viewed at [wileyonlinelibrary.com](http://wileyonlinelibrary.com)]

show a structure with spherulite globular domains. The globular domains are visible for the PU-PURE and PU-DPG, while the PU-MEG and PU-BDO show a substantially smoother surface. Therefore, it indicates that the globular domain varies according to the CE used. Subsequently, phase separation morphology on the surface of each PU was elucidated in more detail by tapping mode AFM.

The PUs morphology with different CEs was visualized by using tapping mode AFM, which allows simultaneous detection of phase and height features. Figure 11 shows Height (left) and phase (right) AFM images of PU-PURE, PU-MEG, PU-BDO, and PU-DPG. In all PUs, the height and phase maps are consistent with SEM results. All PUs with CEs (PU-MEG, PU-BDO, and PU-DPG) have a microstructure with a phase separation degree. The brighter areas in height images correspond to crystalline regions in PUs (hard phase domain) composed by MDI/CE,<sup>46</sup> while the darker areas correspond to the soft phase domain, SOP. By appropriate image processing, one can enhance the contrast between the two phases.<sup>47</sup> The boundaries between the two phases are much better defined in the oscillatory phase images (right) compared to the height images (left) sensitive to material properties.

The AFM phase image is composed of elongated bright structures (yellow - hard phase domain) separated by darker areas (blue - soft phase domain) as proposed in height images. In the PU-DPG (Figure 11(b)), there was not observed a hard domain structure on this scale. DPG is more soluble in both phases, so the domains are more difficult to detect. Although an increase in the amount of

rigid segment in PU-DPG when compared to PU-PURO (Figure 11(c)), in this sample, it was noted the formation of well-defined rigid segments, interspersed with the soft segment. Due to a possible effect that the DPG extender act as a compatibilizer between the segments, an effect for which it was not detectable in FTIR measurements. For PU-BDO (Figure 11(d)), the hard segment dominates, obtaining a structure of hard and brittle PU film. Nevertheless, for all PUs with CEs, the hard domain increased according to the type of chemical structure of each CE. Thus, we conclude that the increase in the hard domain was in line with the increase in the  $-\text{CH}_2-$  sequence in the CE, the larger the  $-\text{CH}_2-$  sequence in a PU, the denser compact structure is obtained,<sup>43</sup> and it can also be associated with the strong inter- and intramolecular interactions of the hydrogen bonds formed during synthesis between the hard domains.<sup>27</sup>

So far, it has been observed that the thermal, dielectric, and morphological properties change according to the CE used for each PU. Thus, domain size, dispersion, and formation of organized phases can be evaluated by WAXD and SAXS. The WAXD and SAXS were merged to elucidate the structure levels in PUs. The Lorentz correction profiles  $I(q)q^2$  versus  $q$  of the desmeared SAXS-WAXD data are plotted on a relative scale and shown in Figure 12. The PUs materials showed correlation peaks ( $q_{1 \text{ max}} \sim 0.6 \text{ nm}^{-1}$ ,  $q_{2 \text{ max}} \sim 5.5 \text{ nm}^{-1}$ , and  $q_{3 \text{ max}} \sim 14.5 \text{ nm}^{-1}$ ) that are characteristic of phase-separated domains and interchain distances.<sup>48</sup> The first peak at  $\sim 0.6 \text{ nm}^{-1}$  is related to the inter-domain average distance around of 10.7 nm computed by Bragg's relation,  $L = 2\pi/q_{i \text{ max}}$ . It has also been noted that PUs with BDO and MEG extenders have a narrower peak, which is domains smaller polydispersion characteristic, whereas with DPG it is broader because it is an isomer. The broad peaks at 5.5 (1.14 nm) and  $14.5 \text{ nm}^{-1}$  (0.43 nm) are typical of the amorphous PU materials.<sup>49,50</sup> PU prepared with CEs, it is noted a small Bragg peak at  $13.2 \text{ nm}^{-1}$  related to the inter-dispersed hard domains formation. Due to the small size and greater regularity of the extender, the PUs synthesized with BDO, DPG and MEG have a higher phase separation degree between the soft and hard domains, according to FTIR and AFM analysis.

## 4 | CONCLUSIONS

In this article, soybean PUs with different CEs was synthesized by the one-shot method. The effect that the different CEs have on the morphological, thermal, and viscoelastic properties of soybean PUs were evaluated. A detailed analysis of the stretching in the carbonyl

region ( $1600\text{--}1800 \text{ cm}^{-1}$ ) of the hard and soft domains is presented through the FTIR. Besides, the MP,  $X_b$ , HP, and  $W_h$  were also calculated. In all PUs with CEs, the MP increased due to an increased crosslinking degree.  $X_b$  showed similar values to those of HP due to the ordering forces coming from the physical chain (dipole-dipole) new interactions in the soft domains. However, hydrogen bond formation contributes to the phase separation degree. The DMA and DRS combination analysis correlated with the mobility response in the mechanical and electrical fields. At low temperature, there are a  $\gamma$ - and  $\beta$ - transitions at  $-111$  and  $-40^\circ\text{C}$ . The  $\gamma$ -transition was due to the group  $-\text{CH}_2-$  rotation motion in the amorphous region. The  $\beta$ -transition was attributed to the smaller group rotation motions in the fatty acid chains. At high temperature, a  $\alpha$ -transition (at  $60^\circ\text{C}$ ) and a MWS relaxation interfacial, related to the build-up of charges at the interfaces of the microphase separation of the soft and hard domains, were also identified. The  $\alpha$ -transition was associated with the segmental motion in the main chain. The  $T_{gS}$  and  $T_{gH}$  also were identified at  $\sim -27$  and  $\sim 50^\circ\text{C}$ , while the SOP has a  $-80^\circ\text{C}$   $T_g$ . The PUs  $T_g$  increase when compared to polyol which indicates that there was a mixing degree between hard and soft domains. In all PUs,  $\gamma$  transition activation energy obtained was similar (around  $30.6 \text{ kJ/mol}$ ). It noted that the CE effect did not influence the activation energy, obeying the Arrhenius behavior. CEs mobility is dependent on the hydrogen bond degree in the hard domains. All PUs with CEs showed a morphology composed of heterogeneous spherulite globular domains. However, the different CEs used generated increased crystallinity in the hard domain structure, making it more compact and organized, which assumed specific conformations according to each CE. Finally, the right consistency between the DMA and DRS results allowed us to significantly improve the knowledge of the molecular structure and dynamic molecular relations. These results set will enable us to improve the PUs knowledge substantially with CEs based on soybean oil.

## ACKNOWLEDGMENTS

The authors thank the financial support from the Brazilian Agency Coordenação de Aperfeiçoamento de Pessoal de Nível Superior (CAPES), and Sindicato das Indústrias de Material Plástico do Nordeste Gaúcho (SIMPLÁS) for the gratification received at Jovens Pesquisadores 2017, da University of Caxias do Sul (UCS). The authors also thank the Brazilian Synchrotron Light Laboratory for use your installation (SAX1 beamline). Carlos A. Figueroa and Otávio Bianchi are National Council for Scientific and Technological Development (CNPq) fellows (grant

number 306086/2018-2). Clara M. Gómez and Maria J. Sanchis thank the Spanish Ministerio de Economía y Competitividad (RTI2018-093711-B-100) for partial financial help. Ana Cros acknowledges financial support from ENE2016-79282-C5-3-R (AEI/FEDER, UE).

#### DATA AVAILABILITY STATEMENT

The raw data needed to reproduce these findings can be shared if requested from the authors.

#### ORCID

Otávio Bianchi  <https://orcid.org/0000-0001-7493-8163>

#### REFERENCES

- [1] C. M. Gomez, D. Gutierrez, A. Nohales, *J. Elastomers Plast.* **2017**, *49*, 77.
- [2] Z. S. Petrović, M. J. Cevallos, I. Javni, D. Schaefer, *J. Polym. Sci. Pol. Phys.* **2005**, *43*, 3178.
- [3] D. L. Agnol, F. T. G. Dias, N. F. Nicoletti, D. Marinowic, S. M. Silva, A. Falavigna, A. Marcos-Fernandez, O. J. Bianchi, *Biomater. Appl.* **2019**, *34*, 673.
- [4] D. Favero, V. R. R. Marcon, T. Barcellos, C. M. Gómez, M. J. Sanchis, M. Carsí, C. A. Figueroa, O. Bianchi, *J. Mol. Liq.* **2019**, *285*, 136. <http://dx.doi.org/10.1016/j.molliq.2019.04.078>.
- [5] G. A. Oertel, Chapter 1. in *Polyurethane Handbook: Chemistry-Raw Materials-Processing- Application-Properties*, Vol. 1, Hanser Publishers, New York, NY **1985**, p. 7.
- [6] S. H. Havriliak, S. Negami, *J. Polym. Sci. C: Polymer Symposia* **1966**, *14*, 99.
- [7] R. H. Boyd, *Int. J. Chem. Phys.* **1961**, *35*, 1281.
- [8] H. Frohlick, Chapter 1. in *Theory of Dielectrics*, Vol. 1, Oxford, London **1956**, p. 34.
- [9] P. A. Ourique, F. G. Ornaghi, H. L. Ornaghi, C. H. Wanke, O. Bianchi, *J. Therm. Anal. Calorim.* **2019**, *137*, 1969.
- [10] S. Allauddin, V. Somiseti, T. Ravinder, R. BVSK, R. Narayan, K. V. S. N. Raju, *Ind. Crop. Prod.* **2016**, *85*, 361.
- [11] Roy, S. G. Novel Approaches for Synthesis of Polyols from Soy Oils. Ph.D. Thesis, University of Toronto, Toronto, CA, June 2010.
- [12] D. M. Bechi, M. A. de Luca, M. Martinelli, S. Mitidieri, *Prog. Org. Coat.* **2013**, *76*, 736.
- [13] S. Allauddin, R. Narayan, K. Raju, *Acs. Sustain. Chem. Eng.* **2013**, *1*, 910. <https://doi.org/10.1021/sc3001756>.
- [14] F. C. Wang, M. Feve, T. M. Lam, J. P. Pascault, *J. Polym. Sci. Pol. Phys.* **1994**, *32*, 1305. <https://doi.org/10.1002/polb.1994.090320801>.
- [15] L. N. Dang, L. H. Sinh, M. Malin, W. Jürgen, M. Schnabelrauch, S. Jukka, *Eur. Polym. J.* **2016**, *81*, 129.
- [16] E. Yilgör, I. Yilgör, E. Yurtsever, *Polymer* **2002**, *43*, 6551.
- [17] A. Niemczyk, A. Piegat, A. S. Olalla, M. El Fray, *Eur. Polym. J.* **2017**, *93*, 182.
- [18] M. Zhao, W. C. Xu, S. Y. Yong, *Int. J. Mech. Mater.* **2014**, *548*, 164.
- [19] P. R. Couchman, L. Korugic-Karasz, *Macromolecules* **1978**, *11*, 117.
- [20] V. Costa, A. Nohales, P. Félix, C. Guillem, D. Gutiérrez, C. M. Gómez, *J. Appl. Polym. Sci.* **2015**, *132*, 41704.
- [21] R. J. Lockwood, L. M. Alberino, *J. Am. Chem. Soc.* **1981**, *23*, 363.
- [22] G. Sauti, D. S. McLachlan, *J. Mater. Sci.* **2007**, *42*, 6477.
- [23] A. Eceiza, M. Martín, G. Kortaberri, N. Gabilondo, M. A. Corcuera, I. Mondragon, K. de la Caba, *Polym. Eng. Sci.* **2008**, *48*, 297.
- [24] D. W. Van Krevelen, K. Te Nijenhuis, Chapter 6. in *Properties of Polymers: Their Correlation with Chemical Structure: Their Numerical Estimation and Prediction from Additive Group Contributions*, Vol. 1, Elsevier, Amsterdã **2009**, p. 129.
- [25] Z. S. Petrović, J. Milić, F. Zhang, J. Ilavsky, *Polymer* **2017**, *121*, 26.
- [26] Z. H. Shah, Q. Tahir, Dielectric properties of vegetable oils *J. Sci. Res.* **2011**, *3*, 481.
- [27] Z. S. Petrović, D. Hong, I. Javni, N. Erina, F. Zhang, J. Ilavský, *Polymer* **2013**, *54*, 372.
- [28] I. Javni, W. Zhang, Z. S. Petrović, *J. Appl. Polym. Sci.* **2003**, *88*, 2912.
- [29] Z. Martin, H. Kahl, B. Schade, T. Rödel, M. Dionisio, M. Beiner, *Polymer* **2017**, *111*, 83.
- [30] M. A. Corcuera, L. Rueda, A. Saralegui, M. D. Martín, B. Fernández-d'Arlas, I. Mondragon, A. Eceiza, *J. Appl. Polym. Sci.* **2011**, *122*, 3677.
- [31] Z. S. Petrović, *Polymer Reviews* **2008**, *48*, 109. <https://doi.org/10.1080/15583720701834224>.
- [32] S. Dworakowska, D. Bogdal, A. Prociak, *Polymer* **2012**, *4*, 1462.
- [33] D. K. Chattopadhyay, B. Sreedhar, K. V. S. N. Raju, *Ind. Eng. Chem. Res.* **2005**, *44*, 1772.
- [34] T. S. Velayutham, W. H. Abd Majid, A. B. Ahmad, G. Kang, S. N. Gan, *Prog. Org. Coat.* **2009**, *66*, 367.
- [35] A. Schönhal, F. Kremer, Chapter 2. in *Broadband Dielectric Spectroscopy*, Vol. 1, Springer, New York, NY **2003**, p. 35.
- [36] V. B. Veronese, R. K. Menger, M. M. D. C. Forte, C. L. J. Petzhold, *Appl. Polym. Sci.* **2011**, *120*, 530.
- [37] J. B. Marion, Chapter 3. in *Classical Dynamics of Particles and Systems Academic*, Vol. 1, Academic Press Inc., New York, NY **1965**, p. 56.
- [38] M. Carsí, M. J. Sanchis, S. Vallejos, F. García, J. M. García, *Polymer* **2018**, *10*, 859.
- [39] B. Redondo-Foj, M. Carsí, P. Ortiz-Serna, M. J. Sanchis, S. Vallejos, F. García, J. M. García, *Macromolecules* **2014**, *47*, 5334.
- [40] P. Ortiz-Serna, R. Diaz-Calleja, M. J. Sanchis, E. Riande, A. F. Martins, L. Visconte, R. Nunes, *J. Non-cryst. Solids* **2011**, *357*, 598.
- [41] D. Dupenne, A. Roggero, E. Dantras, A. Lonjon, T. Pierré, C. J. Lacabanne, *J. Non-cryst. Solids* **2017**, *468*, 46.
- [42] M. J. Sanchis, M. Carsí, C. M. Gómez, P. V. M. Culebras, K. N. Gonzales, F. G. Torres, *Carbohydrate Polymers* **2017**, *157*, 353.
- [43] W. K. Sakamoto, A. F. de Assis, D. K. Das-Gupta, *J. Mater. Sci.* **2003**, *38*, 1465.
- [44] I. Perepechko, Chapter 4: Electrical properties of polymers at low temperature. in *Low-Temperature Properties of Polymers*, Vol. 1, Pergamon Press, New York, NY **2013**, p. 98.
- [45] P. Ortiz-Serna, M. Carsí, B. Redondo-Foj, M. J. Sanchis, M. Culebras, C. M. Gómez, A. Cantarero, *J. Appl. Polym. Sci.* **2015**, *132*, 42007.



- [46] A. Saralegi, L. Rueda, B. Fernández-d'Arlas, I. Mondragon, A. Eceiza, M. A. Corcuera, *Polym. Int.* **2013**, *62*, 106.
- [47] R. Van den Berg, M. H. De Groot, M. A. Van Dijk, E. C. Denley, *Polymer* **1994**, *35*, 5778.
- [48] P. A. Ourique, I. Krindges, C. Aguzzoli, C. A. Figueroa, J. Amalvy, C. H. Wanke, O. Bianchi, *Prog. Org. Coat.* **2017**, *108*, 15.
- [49] G. Lligadas, J. C. Ronda, M. Galià, V. Cádiz, *Bio-macromolecules* **2007**, *8*, 1858.
- [50] I. Javni, O. Bilić, N. Bilić, Z. S. Petrović, E. A. Eastwood, F. Zhang, J. Ilavský, *Polym. Int.* **2015**, *64*, 1607. <https://doi.org/10.1002/pi.4960>.

## SUPPORTING INFORMATION

Additional supporting information may be found online in the Supporting Information section at the end of this article.

**How to cite this article:** Favero D, Marcon V, Figueroa CA, et al. Effect of chain extender on the morphology, thermal, viscoelastic, and dielectric behavior of soybean polyurethane. *J Appl Polym Sci.* 2021;e50709. <https://doi.org/10.1002/app.50709>